Defects in Kesterite Structures and the Impact of Focused Ion Beam Preparation for TEM Analysis

A. Silva-Mendes, T. Kumar, D. Jensen, L. Costa, H. Müller, J. S. Delgado, F. Santos, R. M. Pereira

***Abstract*— Kesterite solar cells based in Cu_2ZnSnS_4 and $Cu_2ZnSnSe_4$ are potential future candidates to be used in thin film solar cells. The technology still has to be developed to a great extent and for this to happen, high levels of confidance in the characterization methods are required so that improvements can be made on solid interpretations. In this study we show that the interpretations of one of the most used characterization techniques in kesterites, scanning transmission electron microscopy (STEM), might be affected by its specimen preparation when using focused ion beam (FIB). Using complementary measurements based on scanning electron microscopy and Raman scattering spectroscopy, compelling evidences show that secondary phases of ZnSe mixed in the bulk of $Cu_2ZnSnSe_4$ are causing the appearance of voids in the STEM lamellae. Sputtering simulations support this interpretation by showing that Zn in a ZnSe matrix is preferentially sputtered compared with any metal atom in a $Cu_2ZnSnSe_4$ matrix.**

***Index Terms*—thin film solar cells, focused ion beam (FIB), transmission electron microscopy (TEM), kesterite, $Cu_2ZnSn(S,Se)_4$ (CZTSSe)**

I. Introduction

The semiconductor $Cu_2ZnSn(S,Se)_4$ (CZTSSe), with kesterite crystalline structure, is currently studied as the absorber layer in thin film solar cells. The biggest selling point of the CZTSSe compound has been the use of abundant materials like Cu, Zn, and Sn [1]. Some other advantages of the CZTSSe compound are: its tuneable bandgap energy from ~1 eV[2], [3] to 1.5 eV[4] (by replacing Se by S); the high value of optical absorption [5], [6]; the use of a solar cell structure similar to the one of $Cu(In,Ga)Se_2$ [7], [8]; some doping properties can be achieved by diffusion of alkalis from the glass[9]; the flexibility in having several methods capable of synthetizing the compound[10]–[18]; just to name a few. In spite of these advantages, the maximum power conversion efficiency of a CZTSSe laboratory solar cell is just around 12.6 %[19]. Such limited efficiency has been attributed to a few issues which significantly limit the open circuit voltage (V_{oc}): secondary phases[20]–[25]; poor band alignments and cell architecture problems[15], [16], [26], [27]; high values of fluctuating potentials [28]–[31] and a kesterite/stannite crystal mixture [32]–[34]. Among all these issues, secondary phases have been intensively studied as they form easily [23], [35]–[37] and are detrimental from an electrical point of view. Raman spectroscopy, X-ray diffraction (XRD), and scanning transmission electron microscopy (STEM) are the most frequently used techniques to identify these spurious phases. In particular, STEM analysis is quite relevant as it allows for an evaluation of the morphology, crystallinity, and of the sample's elemental composition (by energy-dispersive x-ray spectroscopy - EDS). Commonly, the preparation of the STEM lamellae is done either by a combination of mechanical and Ar^+ ion polishing or by milling with a Ga^+ focused ion beam (FIB). State-of-the art FIB tools are capable of sample preparation with the advantage of a fast and precise milling of the lamellae, with a very limited damage to the lamellae surface by finishing the milling with low ion beam energy (0.50 - 2 keV). However, even in these cases the ion milling process might create artefacts in some material systems.

In this work, we present a study that shows that the preparation of STEM specimens by using FIB sample preparation might lead to the appearance of artefacts in the STEM characterization of $Cu_2ZnSnSe_4$ (CZTSe) samples. There is evidence that voids in the lamellae observed in STEM analysis are in fact artefacts created by the presence of ZnSe secondary phases in the CZTSe sample. We use a combination of STEM, Raman spectroscopy, scanning electron microscopy (SEM), and sputtering simulations to support these findings.

II. Experimental

Solar cells were fabricated on a 3 mm thick, 25 cm^2 soda lime glass (SLG) substrate covered by 400 nm of Molybdenum (Mo) as electrical back contact. Metallic precursors were sequentially deposited using e-beam evaporation and selenized at 460 ^oC in a Se-rich atmosphere to form the CZTSe layer as described elsewhere [38]. This particular set of samples had a 100 nm thick SiO_2 layer sputtered on top of the SLG to prevent alkali diffusion [9]. The CZTSe absorbers were then finished into solar cells with a CdS layer deposited by chemical bath deposition and a transparent conductive oxide constituted by i-ZnO and ZnO:Al. The final solar cell structure was: $SLG/SiO_2/Mo/CZTSe/CdS/i\text{-}ZnO/ZnO:Al$ and the device studied here had a power conversion efficiency of 5.3 %. We note that on top of Mo, a layer of $MoSe_2$ is usually formed [39].

Scanning transmission electron microscopy (STEM) images were taken with a FEI Titan ChemiThemis 80-200 kV Cs-probe corrected transmission electron microscope, operating at 200 kV accelerating potential and equipped with electron Bruker EDS SuperX detector. In this method a coherent focused probe scans across the specimen and the X-ray emission spectrum is recorded in each probe position. All samples studied in cross section mode were prepared in a FIB

FEI Dual-Beam Helios 450S with FIB lift-out Mo-grids using a technique known as "lift-out" [40]. On top of the solar cell we deposit a carbon layer to reduce the charging effect that displaces the electron/ion beam during the Pt bi-layer deposition. The Pt deposition assisted by the electron and the Ga beam serves to reduce the vertical ripples (curtain effect or waterfall effect) [41]–[43] due to changes in the sputter yield and angle of incidence as the ion beam passes over a step, pore, local curvature or regions of different compositions. The lamella ion-milling, i.e. the polishing process, was done using a Ga^+ beam with 30 -15 - 2 – 1 kV polishing steps to thin down the lamella and a final polishing energy of 1 kV to minimize lamella surface damage. SEM images were taken with a high-resolution NovaNanoSEM 650 SEM system. Raman scattering experiments were carried out at room temperature using a Jobin-Yvon LabRaman HR800 spectrometer equipped with a multi-channel Peltier cooled CCD detector, in the backscattering geometry, and using a 442 nm excitation wavelength. The sample surface was focused with an objective of 50x (N.A=0.50; WD=10.6 mm), and the incident power was varied from 70 µW to 790 µW.

III. Results

A bright field (BF) cross-section image of the CZTSe lamella is shown in Fig.1. The image shows, from bottom to top, the Mo rear electrode (deposited with 4 layers), a $MoSe_2$ layer, the CZTSe absorber, the CdS buffer layer, the ZnO transparent conductive layers, a thin and bright protective carbon layer and then another protective Pt layer deposited by the FIB. In STEM BF images, bright areas correspond to very low mass density regions (e.g. the protective carbon layer) or to voids/empty spaces where the lamella is highly transparent to the incoming beam. That is the case of the low mass density protective carbon layer. The ZnO layer presents some vertical white segments, corresponding to cracks or pin-holes in the film. Other bright areas or pin-holes can be observed in the CZTSe layer. The identification of such pinholes is important as they are detrimental from a device point of view. The observation of voids in the growth of kesterite materials is something that is common and it has been attributed mostly to Kirkendall effects during the chalcogenation process[44]–[46] and to the complex thermodynamic reactions taking place at the Mo interface [47]. As such, the voids seen in the literature have the tendency to be present close to the back contact. In our case, although voids are present close to the Mo interface, they are also present to some extent throughout the whole thickness of the CZTSe.

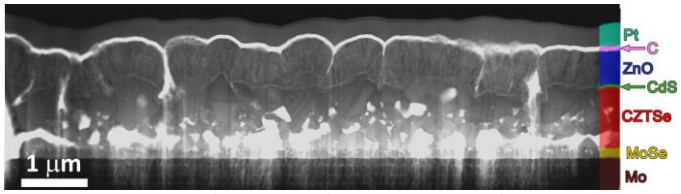

Figure 1: STEM bright field image of the cross section of a CZTSe solar cell. The white spots are voids in the CZTSe film while the top continuous white layer is the protective carbon coating.

To validate the presence of the voids and to analyse the elemental distribution of the sample, we performed high-angle annular dark-field (HAADF) imaging and EDS analysis. Fig 2 a) shows a HAADF image of the same region of the lamella. The voids and the protective carbon layer now show a dark contrast. EDS mappings for Sn, Cu, Zn, Se, Cd, and S for the same region are also presented. Cu and Sn are distributed equally inside the CZTSe but not uniformly, as there are spots without any counts. For the Zn and Se EDS mapping, we can still see dark areas, corresponding to voids, and there is also a high intensity of the Zn and Se signals close to the voids. The high concentration of Zn in the top layers corresponds to the ZnO layer. In the CZTSe layer, a bright spot in the BF image (or dark in the HAADF image) could be related both with a void or with a lower atomic number phase like ZnSe, since Sn (Z=50) is a much heavier element than Cu (Z=29), Zn (Z=30), and Se (Z=34). Thus, a ZnSe region would appear as a much lighter elemental region than a $Cu_2SnZnSe_4$ region. The EDS analysis shows that parts of the dark regions in the HAADF image are indeed Zn-rich areas and it also shows that close to these regions, there are areas with no EDS signal of any element, confirming the presence of voids. The non-uniform distribution of Zn and Se with the presence of ZnSe aggregates close to the voids is the first indication that the two events can be to a certain degree correlated. Furthermore, the EDS analysis also shows that a small number of the visible voids are surrounded by Cd and S, suggesting a layer of CdS. This fact can be explained by these specific voids being already present during the chemical bath deposition of the CdS layer. On the voids where Cd and S are present, the concentration of Zn is similar to the rest of the film. Hence, this analysis reveals the possibility of two different type of voids: i) voids that were already present at the sample preparation stage and that were identified by being coated by a CdS layer; ii) voids that are close to the segregation of ZnSe aggregates. In the rest of the manuscript, we will focus our attention to the second type of voids.

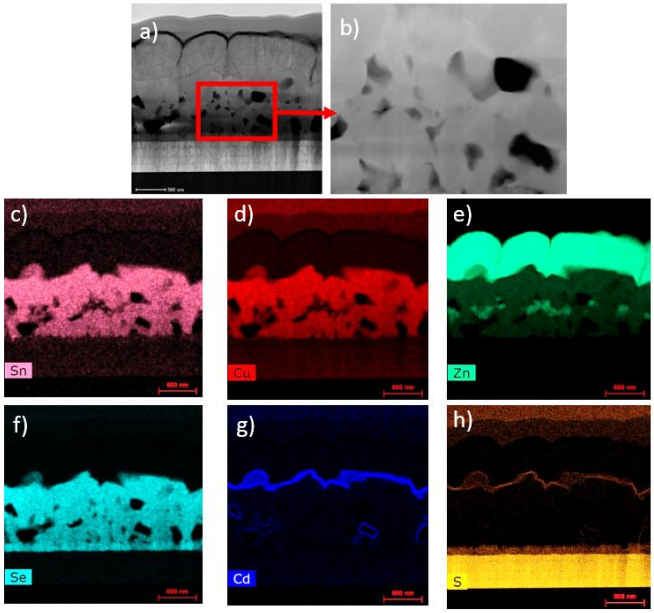

Figure 2: a) and b) HAADF image and corresponding STEM-EDS maps for c) Sn, d) Cu, e) Zn, f) Se, g) Cd and h) S. The analysis confirms voids in the sample with a slight enrichment of ZnSe in adjacent regions. The high concentration of S at the back contact is due to superimposition with Mo.

To verify if the voids that are not coated in CdS are present in the samples prior to the FIB process, we prepared cross-sections by cleaving the samples and performing SEM measurements. A representative image of the cross-section is shown in Fig. 3. The image shows the same layers as previously but surprisingly, the presence of voids, compared with the STEM images, is significantly reduced. A very small number of what might be voids is present close to the Mo interface. However, contrary to the STEM observations voids are only observed at the grain boundaries of the CZTSe grains. These large CZTSe grains present a dimension similar to the film thickness. Additionally, small grains around the middle of the film with a brighter contrast can be seen. The contrast difference suggests a different chemical composition in the bright grains. Even though the identification of voids using SEM is much more complex due to the fracture process, this basic analysis indicates that the voids observed in the TEM analysis are not present prior to the FIB preparation.

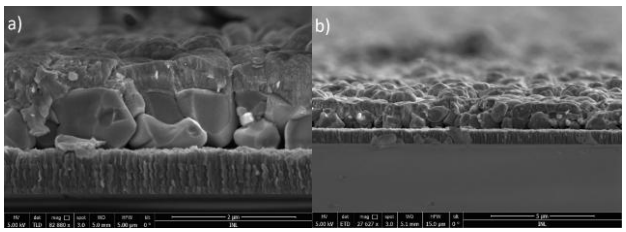

Figure 3: High and low magnification SEM images of the cross-section of the CZTSe solar cell.

As an additional evidence of the appearance of voids during the lamella preparation, we present in figure 4, four SEM images that show the voids formation during the lamella thinning-down process for a second lamella prepared from the same CZTSe sample. After a 30 kV thinning some voids are already visible, as shown in figure 4 a). As discussed previously, some of these voids could already be present in the film. As the thinning-down process progresses, the images show the appearance of more voids as well as their increase in size even for the stages where a lower acceleration voltage is used, figure 4 b), c), and d).

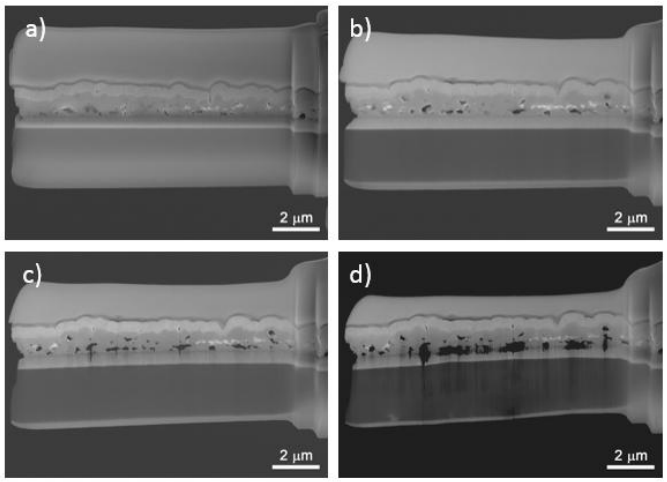

Figure 4: Evolution of the lamella with the thinning-down process at several acceleration voltage stages. a) and b) show the evolution during the 30 kV stage, c) after the 2 kV stage, and d) the final result after a 1 kV polishing stage.

Additionally, we performed Raman scattering spectroscopy, as by XRD, CZTSe cannot be distinguished from ZnSe. The analysis was performed after a standard 1 minute 5 % HCl chemical etch process to remove the ZnO layers and most of the CdS so that most of the absorber layer could be probed. The Raman spectra taken on the surface (Fig. 5a) show peaks at 174, 195, and 233 cm^{-1} corresponding to CZTSe, and at 300 cm^{-1} related to CdS, the latter showing an incomplete etching process of the CdS layer. However, the Raman spectroscopy analysis is only capable of probing down to a few hundred nanometres from the top surface due to the high light absorption coefficient of CZTSe [20], [48]. Hence, we also performed an analysis on the cross-section to probe the full thickness. This kind of analysis is quite complex as the laser spot size is on the same order of magnitude as the film thickness itself, and thus, the volume probed is higher than the effective film volume with a compromise in signal to noise level. The results are seen in Figure 5 b) confirming the presence of the CZTSe phase, as expected, but now ZnSe is also visible with peaks at 250 cm^{-1} and 500 cm^{-1} [20]. The conjugation of both measurements allows us to conclude that ZnSe is present in the depth of the CZTSe film but not at the film´s surface. Thus, the Raman spectroscopy analysis supports the EDS interpretation that the CZTSe sample has ZnSe segregates. It is also important to note that neither voids seen by the STEM nor ZnSe phases seen by Raman spectroscopy were identified at the surface of the sample. Hence, this is a further indication that the voids and the ZnSe segregates are related.

To validate if the appearance of the voids is related with Zn-rich segregates, a lamella of a second CZTSe solar cell fabricated withy optmized conditions that minimize the appearance of secondary phases was prepared by FIB following the same protocol and analyzed similarly [49]. For this optimized fabrication process, the amount of secondary phases is smaller [49]. In Figure 6, the bright field image of the cross-section is presented and, compared with the previous sample, the number of observable voids is dramatically reduced. The HAADF image confirms this observation. EDS mapping of Zn, shown in figure 6 c), shows no segregation. Hence, when there is a reduced number of ZnSe segregates, there is also a reduced number of voids in the TEM lamella.

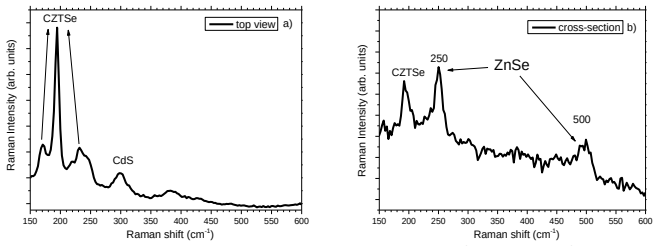

Figure 5: Raman scattering spectroscopy analysis of the a) surface and b) cross-section of a CZTSe sample. The surface measurement shows only the presence of CZTSe and CdS, whereas the cross-section reveals the appearance of ZnSe.

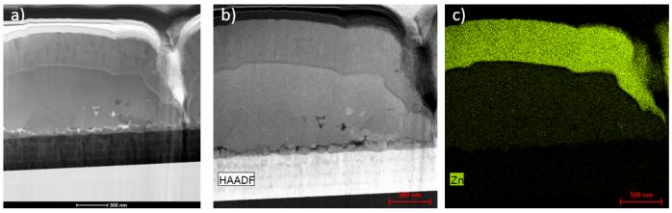

Figure 6: a) BF image of the cross-section of a CZTSe solar cell with reduced number of secondary phases. b) HAADF of the same area and c) EDS mapping of Zn showing no segregation.

Having demonstrated a correlation between the ZnSe aggregates in the EDS analysis close to the voids and the presence of ZnSe secondary phases in the bulk of the CZTSe absorber, we now try to explain why the voids appear during the FIB lamella preparation. At this point, we note that the presence of ZnSe as a secondary phase is largely reported in the literature as it depends on the growth conditions of the CZTSe layer[50]–[52]. We simulated the sputtering yield of the different elements involved when a 30 kV Ga ion beam is incident at a 3º angle, to simulate the effects of the beam tail, using the *Stopping and Range of Ions in Matter* (SRIM) software. The results are summarized in table 1 and, basically, in a solid mixture of Cu-Zn-Sn-Se with ZnSe, an incident Ga^+ beam with an energy of 30 kV sputters away around 4 times more Zn if it hits ZnSe compared with the same beam hitting CZTSe. Thus, if a compound is constituted by a mixture of CZTSe and ZnSe, a bombardment of Ga^+ ions will sputter away Zn in the ZnSe phase 4 times more efficiently than Zn in the CZTSe phase. This observation is true both for 30 kV and 1 kV. It is then evident that during the FIB thinning-down process of the CZTSe lamella, the presence of a ZnSe secondary phase leads to the appearance of voids as the ZnSe secondary phases are sputtered preferentially. While a realistic simulation of the lamella milling accounting for material re-deposition [53], ion beam tails [54] ion channeling[55], [56] and other [42], [43] issues that can influence the formation of voids is a very complicated task, our simple modelling fits and explains well the observed results. The exact reason why part of the ZnSe aggregates are sputtered away while some minor ZnSe phases stays close to the voids could be explained by a non 3-dimensional uniformity of the phase distribution but again, these simulations are complex and it is intuitive to understand that a surface sputtering of a non-uniform 3D thin film can lead to several effects.

Table 1: Average number of sputtered atoms when a Ga ion with energy of 30 kV and 1 KV strikes a solid mixture of Zn; ZnSe and CZTSe.

	Compound	Zn	Se	Sn	Cu
Ga ion beam at 30 kV	ZnSe	23.4	15.0	-	-
	CZTSe	6.0	15.6	2.6	5.3
Ga ion beam at 1 kV	ZnSe	3.2	2.0	-	-
	CZTSe	0.8	2.1	0.3	0.8

IV. CONCLUSIONS

In this work we identified two different types of voids seen in TEM lamellas. The first type are natural occurring voids that are evenly coated by CdS during the chemical bath deposition and that are present in the early stages of the FIB preparation and in SEM cross-section images. These voids are usually attributed to Kirkendall effects [44]–[46]. The second type of voids, larger and present with a higher amount compared with the natural occurring voids, are the likely results of the FIB preparation of CZTSe TEM lamellae. Our results clearly show that the presence of ZnSe segregates can lead to voids during the FIB milling. This conclusion is supported by several characterizations performed. Firstly, an increased amount of ZnSe close to the voids was seen by the EDS analysis. Secondly, cross-section images taken during the thinning-down process, clearly show an increase in both size and number of voids in the CZTSe film. Thirdly, the void formation can be explained by simple sputtering simulations that show a preferential sputtering of ZnSe versus CZTSe, with 4 times higher sputtering efficiency for ZnSe. Fourthly, a CZTSe sample that was intentionally optimized and prepared with a lower concentration of ZnSe secondary phases, shows almost no voids. Hence, the observation of voids in kesterite samples using TEM analysis has to be taken with care if the preparation of the lamellae is done using FIB. In fact, several works found voids and local excess of Zn(S,Se) [57]–[60], which are the main indications of the artefacts found in our study. TEM studies have to be paired with other analysis in order to have complementary data. A suggestion is to document the FIB thinning-down process with SEM images and EDS mapping, a process which, unfortunately, is very elaborate. We note that even for TEM specimen prepared with other means, the artefacts can also appear since most of them also use ion-based polishing steps. We note that the findings of this work might not be universal for kesterites as many factors and properties influence the sputtering properties of the FIB preparation, specifically for this material where its properties are heavily influenced by its preparation method. Examples of these properties are: grain boundaries and differences in orientation; different types of segregations and secondary phases; elemental depth and lateral profiling; pre-existence of other features as voids or differences in density. Hence, only a very complex analysis that would include these conditions would allow one to understand the full effect of the FIB sputtering on the sample preparation. However, the use of more advanced preparation techniques with cryo steps or rocking approaches could also be a solution to the found artefacts.

REFERENCES

[1] J. J. Scragg, P. J. Dale, L. M. Peter, G. Zoppi, and I. Forbes, "New routes to sustainable photovoltaics: Evaluation of Cu_2ZnSnS_4 as an alternative absorber material," *Phys. Status Solidi Basic Res.*, vol. 245, no. 9, pp. 1772–1778, 2008.

[2] P. M. P. Salomé *et al.*, "Growth pressure dependence of $Cu_2ZnSnSe_4$ properties," *Sol. Energy Mater. Sol. Cells*, vol. 94, no. 12, pp. 2176–2180, 2010.

[3] A. Walsh, S. H. Wei, S. Chen, and X. G. Gong, "Design of quaternary chalcogenide photovoltaic absorbers through cation mutation," *Conf. Rec. IEEE Photovolt. Spec. Conf.*, pp. 001875–001878, 2009.

[4] K. Sekiguchi, K. Tanaka, K. Moriya, and H. Uchiki, "Epitaxial growth of Cu_2ZnSnS_4 thin films by pulsed laser deposition," *Phys. Status Solidi*, vol. 3, no. 8, pp. 2618–2621, 2006.

[5] C. Persson, "Electronic and optical properties of Cu_2ZnSnS_4 and $Cu_2ZnSnSe_4$," *J. Appl. Phys.*, vol. 107, no. 5, pp. 1–8, 2010.
[6] K. Ito and T. Nakazawa, "Electrical and optical properties of Stannite-type quaternary semiconductor thin films." pp. 2094–2097, 1988.
[7] P. A. Fernandes, P. M. P. Salomé, A. F. Da Cunha, and B. A. Schubert, "Cu_2ZnSnS_4 solar cells prepared with sulphurized dc-sputtered stacked metallic precursors," *Thin Solid Films*, vol. 519, no. 21, pp. 7382–7385, 2011.
[8] J. Li *et al.*, "Tailoring the defects and carrier density for beyond 10% efficient CZTSe thin film solar cells," *Sol. Energy Mater. Sol. Cells*, vol. 159, no. August 2016, pp. 447–455, 2017.
[9] P. M. P. Salomé, H. Rodriguez-Alvarez, and S. Sadewasser, "Incorporation of alkali metals in chalcogenide solar cells," *Sol. Energy Mater. Sol. Cells*, vol. 143, pp. 9–20, 2015.
[10] P. K. Sarswat, M. Snure, M. L. Free, and A. Tiwari, "CZTS thin films on transparent conducting electrodes by electrochemical technique," *Thin Solid Films*, vol. 520, no. 6, pp. 1694–1697, 2012.
[11] P. K. Sarswat and M. L. Free, "A Comparative study of co-electrodeposited Cu_2ZnSnS_4 absorber material on fluorinated tin oxide and molybdenum substrates," *J. Electron. Mater.*, vol. 41, no. 8, pp. 2210–2215, 2012.
[12] P. K. Sarswat and M. L. Free, "An investigation of rapidly synthesized Cu_2ZnSnS_4 nanocrystals," *J. Cryst. Growth*, vol. 372, pp. 87–94, 2013.
[13] K. Tanaka, Y. Takamatsu, and S. Miura, "Chemical composition dependence of photoluminescence from Cu_2ZnSnS_4 thin films with potential fluctuations," *Phys. Status Solidi*, vol. 1600138, 2017.
[14] J. Poortmans *et al.*, "Progress in Cleaning and Wet Processing for Kesterite Thin Film Solar Cells," *Ultra Clean Process. Semicond. Surfaces XIII*, vol. 255, pp. 348–353, 2016.
[15] M. Courel, E. Valencia-Resendiz, J. A. Andrade-Arvizu, E. Saucedo, and O. Vigil-Galán, "Towards understanding poor performances in spray-deposited Cu_2ZnSnS_4 thin film solar cells," *Sol. Energy Mater. Sol. Cells*, vol. 159, pp. 151–158, 2017.
[16] C. Platzer-Björkman *et al.*, "Reduced interface recombination in Cu_2ZnSnS_4 solar cells with atomic layer deposition Zn1-xSnxOy buffer layers," *Appl. Phys. Lett.*, vol. 107, no. 24, pp. 1–5, 2015.
[17] M. T. Winkler, W. Wang, O. Gunawan, H. J. Hovel, T. K. Todorov, and D. B. Mitzi, "Optical designs that improve the efficiency of $Cu_2ZnSn(S,Se)_4$ solar cells," *Energy Environ. Sci.*, vol. 7, no. 3, pp. 1029–1036, 2014.
[18] I. Repins *et al.*, "Co-evaporated $Cu_2ZnSnSe_4$ films and devices," *Sol. Energy Mater. Sol. Cells*, vol. 101, pp. 154–159, 2012.
[19] W. Wang *et al.*, "Device characteristics of CZTSSe thin-film solar cells with 12.6% efficiency," *Adv. Energy Mater.*, vol. 4, no. 7, pp. 1–5, 2014.
[20] P. M. P. Salomé, P. A. Fernandes, J. P. Leitão, M. G. Sousa, J. P. Teixeira, and A. F. da Cunha, "Secondary crystalline phases identification in $Cu_2ZnSnSe_4$ thin films: contributions from Raman scattering and photoluminescence," *J. Mater. Sci.*, vol. 49, no. 21, pp. 7425–7436, 2014.
[21] P. A. Fernandes, P. M. P. Salomé, and A. F. da Cunha, "Growth and Raman scattering characterization of Cu2ZnSnS4 thin films," *Thin Solid Films*, vol. 517, no. 7, pp. 2519–2523, 2009.
[22] B. Vermang *et al.*, "Rear surface optimization of CZTS solar cells by use of a passivation layer with nanosized point openings," *IEEE J. Photovoltaics*, vol. 6, no. 1, pp. 332–336, 2016.
[23] H. Xie *et al.*, "Impact of Sn (S, Se) Secondary Phases in $Cu_2ZnSn(S, Se)_4$ Solar Cells: a Chemical Route for Their Selective Removal and Absorber Surface Passivation," *ACS Appl. Mater. Interfaces*, vol. 6, no. 15, pp. 12744–12751, 2014.
[24] A. Kanevce, I. Repins, and S. H. Wei, "Impact of bulk properties and local secondary phases on the $Cu_2(Zn,Sn)Se_4$ solar cells open-circuit voltage," *Sol. Energy Mater. Sol. Cells*, vol. 133, pp. 119–125, 2015.
[25] R. Ahmad *et al.*, "A comprehensive study on the mechanism behind formation and depletion of Cu 2 ZnSnS 4 (CZTS) phases," *CrystEngComm*, vol. 17, no. 36, pp. 6972–6984, 2015.
[26] S. Garud *et al.*, "Alkali Assisted Reduction of Open-Circuit Voltage Deficit in CZTSe Solar Cells," in *Physica Status Solidi (C) Current Topics in Solid State Physics*, 2017, vol. 14, no. 10, pp. 2–7.
[27] J. Kim, S. Park, S. Ryu, J. Oh, and B. Shin, "Improving the open-circuit voltage of $Cu_2ZnSnSe_4$ thin film solar cells via interface passivation," *Prog. Photovoltaics Res. Appl.*, vol. 25, no. 4, pp. 308–317, Apr. 2017.
[28] J. P. Teixeira *et al.*, "Comparison of fluctuating potentials and donor-acceptor pair transitions in a Cu-poor Cu_2ZnSnS_4 based solar cell," *Appl. Phys. Lett.*, vol. 105, no. 16, p. 163901, Oct. 2014.
[29] J. P. Teixeira *et al.*, "Radiative transitions in highly doped and compensated chalcopyrites and kesterites: The case of Cu_2ZnSnS_4," *Phys. Rev. B*, vol. 90, no. 23, p. 235202, Dec. 2014.
[30] T. Gokmen, O. Gunawan, T. K. Todorov, and D. B. Mitzi, "Band tailing and efficiency limitation in kesterite solar cells," *Appl. Phys. Lett.*, vol. 103, no. 10, Sep. 2013.
[31] C. J. Hages, N. J. Carter, and R. Agrawal, "Generalized quantum efficiency analysis for non-ideal solar cells: Case of $Cu_2ZnSnSe_4$," *J. Appl. Phys.*, vol. 119, no. 1, 2016.
[32] T. Gershon *et al.*, "Unconventional kesterites: The quest to reduce band tailing in CZTSSe," *Curr. Opin. Green Sustain. Chem.*, vol. 4, pp. 29–36, 2017.
[33] J. J. S. Scragg *et al.*, "Cu-Zn disorder and band gap fluctuations in Cu2ZnSn(S,Se)4: Theoretical and experimental investigations," *Phys. Status Solidi Basic Res.*, vol. 253, no. 2, pp. 247–254, 2016.
[34] G. Rey *et al.*, "The band gap of $Cu_2ZnSnSe_4$: Effect of order-disorder," *Appl. Phys. Lett.*, vol. 105, no. 11,

2014.
[35] H. Katagiri *et al.*, "Enhanced conversion efficiencies of Cu2ZnSnS4-based thin film solar cells by using preferential etching technique," *Appl. Phys. Express*, vol. 1, no. 4, pp. 0412011–0412012, 2008.
[36] C. Wang *et al.*, "Design of I 2 − II − IV − VI 4 Semiconductors through Element Substitution : The Thermodynamic Stability Limit and Chemical Trend," *Chem. Mater.*, vol. 26, pp. 3411–3417, 2014.
[37] M. Kumar, A. Dubey, N. Adhikari, S. Venkatesan, and Q. Qiao, "Strategic review of secondary phases, defects and defect-complexes in kesterite CZTS–Se solar cells," *Energy Environ. Sci.*, vol. 8, no. 11, pp. 3134–3159, 2015.
[38] S. Ranjbar *et al.*, "Effect of Sn/Zn/Cu precursor stack thickness on two-step processed kesterite solar cells," *Thin Solid Films*, vol. 633, pp. 127–130, 2017.
[39] J. Li *et al.*, "A temporary barrier effect of the alloy layer during selenization: Tailoring the thickness of $MoSe_2$ for efficient $Cu_2ZnSnSe_4$ solar cells," *Adv. Energy Mater.*, vol. 5, no. 9, 2015.
[40] S. Bals, W. Tirry, R. Geurts, Z. Yang, and D. Schryvers, "High-Quality Sample Preparation by Low kV FIB Thinning for Analytical TEM Measurements," *Microsc. Microanal.*, vol. 13, no. 02, pp. 80–86, Apr. 2007.
[41] C. A. Volkert, A. M. Minor, and G. Editors, "Focused Ion Beam Micromachining," vol. 32, no. May 2007, pp. 389–399, 2007.
[42] T. Ishitani, K. Umemura, T. Ohnishi, T. Yaguchi, and T. Kamino, "Improvements in performance of focused ion beam cross-sectioning: Aspects of ion-sample interaction," *J. Electron Microsc. (Tokyo).*, vol. 53, no. 5, pp. 443–449, 2004.
[43] L. A. Giannuzzi and F. A. Stevie, Eds., *Introduction to Focused Ion Beams*. Boston, MA: Springer US, 2005.
[44] C. Yan, K. Sun, F. Liu, J. Huang, F. Zhou, and X. Hao, "Boost Voc of pure sulfide kesterite solar cell via a double CZTS layer stacks," *Sol. Energy Mater. Sol. Cells*, vol. 160, no. August 2016, pp. 7–11, 2017.
[45] S. W. Fu, H. J. Chen, S. H. Wu, H. T. Wu, and C. F. Shih, "Impact of pre-alloying of sputtered Cu/Sn/Zn precursors for Cu_2ZnSnS_4 thin films," *Mater. Lett.*, vol. 173, pp. 1–4, 2016.
[46] H. J. Chen, S. W. Fu, S. H. Wu, T. C. Tsai, H. T. Wu, and C. F. Shih, "Impact of SnS Buffer Layer at Mo/Cu_2ZnSnS_4 Interface," *J. Am. Ceram. Soc.*, vol. 99, no. 5, pp. 1808–1814, 2016.
[47] J. J. Scragg, T. Kubart, J. T. Wätjen, T. Ericson, M. K. Linnarsson, and C. Platzer-Björkman, "Effects of back contact instability on Cu_2ZnSnS_4 devices and processes," *Chem. Mater.*, vol. 25, no. 15, pp. 3162–3171, 2013.
[48] X. Fontań *et al.*, "In-depth resolved Raman scattering analysis for the identification of secondary phases: Characterization of Cu_2ZnSnS_4 layers for solar cell applications," *Appl. Phys. Lett.*, vol. 98, no. 18, pp. 4–6, 2011.
[49] S. Sahayaraj *et al.*, "Doping of $Cu_2ZnSnSe_4$ solar cells with Na+ or K+ alkali ions," *J. Mater. Chem. A*, vol. 6, pp. 2653–2663, 2018.
[50] Y.-C. Lin, L.-C. Wang, K.-T. Liu, Y.-R. Syu, and H.-R. Hsu, "A comparative investigation of secondary phases and $MoSe_2$ in $Cu_2ZnSnSe_4$ solar cells: Effect of Zn/Sn ratio," *J. Alloys Compd.*, vol. 743, pp. 249–257, Apr. 2018.
[51] Y. Wei *et al.*, "An investigation on phase transition for as-sputtered $Cu_2ZnSnSe_4$ absorbers during selenization," *Sol. Energy*, vol. 164, pp. 58–64, Apr. 2018.
[52] R. Sun *et al.*, "Beyond 11% efficient $Cu_2ZnSn(Se,S)_4$ thin film solar cells by cadmium alloying," *Sol. Energy Mater. Sol. Cells*, vol. 174, pp. 494–498, Jan. 2018.
[53] J. M. Cairney and P. R. Munroe, "Redeposition effects in transmission electron microscope specimens of FeAl-WC composites prepared using a focused ion beam," *Micron*, vol. 34, no. 2, pp. 97–107, 2003.
[54] C. Lehrer, L. Frey, S. Petersen, and H. Ryssel, "Limitations of focused ion beam nanomachining," *J. Vac. Sci. Technol. B Microelectron. Nanom. Struct.*, vol. 19, no. 6, p. 2533, 2001.
[55] J. C. Gonzalez, D. P. Griffis, T. T. Miau, and P. E. Russell, "Chemically enhanced focused ion beam micromachining of copper," *J. Vac. Sci. Technol. B Microelectron. Nanom. Struct.*, vol. 19, no. 6, pp. 2539–2542, 2001.
[56] J. C. Gonzalez, M. I. N. da Silva, D. P. Griffis, and P. E. Russell, "Improvements in focused ion beam micromachining of interconnect materials," *J. Vac. Sci. Technol. B Microelectron. Nanom. Struct.*, vol. 20, no. 6, p. 2700, 2002.
[57] W. Li, J. Chen, C. Yan, F. Liu, and X. Hao, "Transmission electron microscopy analysis for the process of crystallization of Cu_2ZnSnS_4 film from sputtered Zn/CuSn precursor," *Nanotechnology*, vol. 25, no. 19, p. 195701, 2014.
[58] S. Bag, O. Gunawan, T. Gokmen, Y. Zhu, and D. B. Mitzi, "Hydrazine-processed Ge-substituted CZTSe solar cells," *Chem. Mater.*, vol. 24, no. 23, pp. 4588–4593, 2012.
[59] K. Woo *et al.*, "Band-gap-graded $Cu_2ZnSn(S_{1-x},Se_x)4$ Solar Cells Fabricated by an Ethanol-based, Particulate Precursor Ink Route," *Sci. Rep.*, vol. 3, no. 1, p. 3069, 2013.
[60] J. W. Cho, A. Ismail, S. J. Park, W. Kim, S. Yoon, and B. K. Min, "Synthesis of Cu_2ZnSnS_4 thin films by a precursor solution paste for thin film solar cell applications," *ACS Appl. Mater. Interfaces*, vol. 5, no. 10, pp. 4162–4165, 2013.